IJISET - International Journal of Innovative Science, Engineering & Technology, Vol. 8 Issue 5, May 2021
ISSN (Online) 2348 – 7968 | Impact Factor (2020) – 6.72
www.ijiset.com

Large Eddy Simulation of Nanofluid Turbulent Heat Transfer in a Rectangular Channel have grooves

Ali Sulieman[1,*], Amir Sultan[1], Younes Najim[1]

[1]Mechanical Engineering department, College of Engineering, University of Mosul

*ali.enp64@student.uomosul.edu.iq

Abstract
A comprehensive investigation applying LES (Large-eddy simulation) mode of nanofluid (Al2O3/Water) turbulent heat transfer in a rectangular channel has grooves is performed. The simulation adopts FLUENT-based control volume to solve the turbulent flow field and the associated thermal behavior of the different configurations of the channels. The wall-adopting local eddy-viscosity model is utilized in dealing with the sub-grid scale stress tensor and heat flux vector. The periodic boundary condition is imposed on the streamwise and spanwise directions, while the no-slip and constant heat flux are applied to the walls. The results indicate that adding nanoparticles into the base fluid increases the dimensionless mean velocity and fluctuations of velocity and temperature. This increment is more evident in turbulent Reynolds stress in the streamwise direction than the other directions. Therefore, higher energy is transferred between nanofluid layers which results in a higher amount of heat transfer than the pure water.

1. Introduction

In recent decades, the development in the technological field has led to investigating for new ways to improve heat transfer and obtain high-efficiency, non-consuming, and less-weight thermal systems. There are three methods used for enhancement heat transfer and these are a passive method, active method and compound method. The passive technique has many advantages such as doesn't need any external energy, low cost, easy production, and installation, that made it widely used in many applications by many researchers. usually, the passive method utilizes geometry refinement and fluid additives, geometry refinements such as inserts ribs and rough surface are employed to enhance fluid mixing and the turbulence in the flow, fluid additives like nanofluid. Nanofluids are a novel class of fluid which contains nano-particles (1-100 nm) suspended in a popular fluid such as water, oil, or ethylene glycol. Nano-material used to create a nanofluid involve metallic particles, oxide particles, carbon nanotubes, graphene nano-flakes and ceramic particles, that will increase thermal conduction and heat transfer coefficients of the base fluid ([1–6]). Duangthongsuk & Wongwises [7] studied experimentally the effect of turbulent TiO_2-water nanofluid flow inside a horizontal double-tube counter-flow heat exchanger on the heat transfer coefficient and friction factor. They found that increased Reynolds number and particle concentrations led to increased heat transfer coefficient and pressure drop, improvement of the heat transfer coefficient were approximately 26% greater than that of base-fluid. Mehrjou et al. [8] have experimentally investigated the convection heat transfer of CuO / water nanofluid flow in a square duct under turbulent flow condition. Their results indicate that increase concentration of volume fraction of nanoparticles in nanofluid from 0.2% to 0.5% cause to grow in heat transfer coefficient about 10.34%.

In everyday life, almost all of the flows are turbulent, for example, the flow over aircraft wings, turbine blades, cars, and also flows through large pipes and channels. It is crucial to comprehend what is a turbulent flow for developing adequate models for energy-efficient applications. to deal with the turbulent flow of nanofluid, numerical modelling and simulation have progressively been developed. Parsaiemehr et al. [9]they examined the effect of rectangular ribs in a different angle on the heat transfer of turbulent nanofluid flow inside a rectangular duct. they have used K-w SST model to computed the turbulent eddy viscosity. results revealed that the rate of heat transfer improvement when change volume fractions between 0 to 4% and attack angles from 0 to 60 are 2, 2.2, 2.4 times, respectively. Amani et al. [10] have employed two-phase mixture model for estimation of flow and heat transfer performance of SiO2/water nanofluids under turbulent flow regime. They took into consideration the heterogeneity of the nanoparticles

into the base fluid and the influence of shear rate, viscosity gradient, thermophoresis and Brownian motion on the diffusion of the nanoparticles. They have applied the k-e turbulent model to model turbulent flow. Finally, they found that the impact of the concentration of the volume fraction of nanoparticles on the Nusselt number is more remarkable at lower Re due to an insignificant effect of the flow momentum on the heat transfer.

As shown above, many researchers have conducted several studies using the Reynolds-averaged Navier–Stokes (RANS) based models to simulate the turbulent convective heat transfer of nanofluids. Although most numerical results obtained from the implementation of Navier-Stokes (RANS) mean Reynolds somewhat correspond to the available experimental data. All scales (from Kolmogorov's scales to large scales) are modelled in the RANS-based models. The large-scale flow structures can be captured by the unsteady RANS (URANS). Even although the URANS models display some large-scaled structures in the highly unstable regions, they miss capturing a considerable range of these structures [11]. Bazdidi-Tehrani et al. [12] have checked the degree of correctness of the scale-adaptive simulation (SAS) approach versus the RANS-based models to predict the turbulent mixed convection of nanofluids through a vertical square duct. Results show that the SAS approach can predict the unsteady flow and heat transfer of nanofluids more accurately than the RANS-based models. Otherwise, the method of large eddy simulation (LES) introduces the concept of solution to the discrete filtered governing equations using computational fluid dynamics [13,14]. The motion is separated into small and large scales, often by spatially filtering the velocity field with a kernel, GΔ(x)[15]. with the last ameliorate in the technology of computing power, Large-eddy simulation showing the possibility to improve both the knowledge the reliability of flow solver predictions and the complex physics. While the URANS models dampened out the resolved scales rapidly, the large eddy simulation approach permits the formation of a turbulent spectrum by modifying its length-scale to the resolved structures. Therefore, this approach gives an advantage of the determination of the unsteady turbulent flow and heat transfer fluctuations in all direction of flow.

In this presented study we utilized LES model to describe heat behavior and turbulent flow for nanofluid (Al2O3/Water) through a rectangular channel. The upper and lower walls of the channel are supplied with constant heat flux, the lower surface has grooves while the upper one is flat. The Ansys Fluent 2019 R1 employed and the finite volume method was used to solve the governing equations. The present results of LES are compared and validated against the direct numerical simulation (DNS) data of Moser et al [16]. n terms of the dimensionless mean velocity profile and dimensionless root-mean-square (RMS) of the three velocity components fluctuations. In addition, the effect of additional nanoparticles of Al2O3 to the pure water in different concentrations (0%-4%) with Reynolds (7000) numbers on the heat transfer and turbulent flow inside a rectangular channel has two cases first case straight channel and the second case have various grooves in the bottom wall is studied in this article.

2. Mathematical modeling

2.1 Governing equations

The equations governing for incompressible flow, three-dimensional, unsteady, are the well-known as Navier-Stokes equations, which represent conservation of mass, momentum and energy

$$\frac{\partial u_i}{\partial x_i} = 0 \quad (1)$$

$$\rho_{eff}\left(\frac{Du_i}{Dt}\right) = -\frac{\partial P}{\partial x_i} + \frac{\partial}{\partial x_j} \quad (2)$$

$$\rho_{eff}\left(\frac{Dh}{Dt}\right) = \frac{\partial}{\partial x_j}\left(k_{eff}\frac{\partial T}{\partial x_j}\right) \quad (3)$$

$$\frac{D}{Dt} = \left(\frac{\partial}{\partial t} + u_j\frac{\partial}{\partial x_j}\right) \quad (4)$$

$$h = C_{pnf}T \quad (5)$$

In equation (3) h is the enthalpy of nanofluid and it is equal to:

The essential idea behind large eddy simulation is to segregate each field variable into large-scales and small-scales using a filtering operation. The filtering process successfully filters out the eddies whose scales are smaller than the filter width or grid spacing used in the computations.

The solids have thermophysical properties higher than classical heat transfer fluids such as water. Scattering of the nanoparticles of solids in a cooling fluid can enhance the inherently low thermophysical

properties of the cooling fluid. We adopted the single-phase manner to analyze the thermal and fluid dynamic behavior of the Al2O3/water nanofluid. Researchers have proposed several correlations for calculating thermophysical properties of nanofluids depending on both properties of base fluid and nanoparticles and according to them, several models have been proposed. Nanofluid density is obtained by measuring the volume and weight of the mixture.

The following equations are used to estimate the density and specific heat capacity of the nanofluid (Bock Choon Pak, 2013)[19].

$$\rho_{eff} = (1-\varphi)\rho_{bf} + \varphi\rho_p \quad (6)$$

Where ρ_{bf} and ρ_p are the densities of base-fluid and nanoparticles, respectively.

2.1.1 Heat capacity of nanofluid

Specific heat can find from this equation (Adriana, 2012) [20].

$$C_{peff} = \frac{(1-\varphi)(\rho c_p)_{bf} + \varphi(\rho c_p)_p}{(1-\varphi)\varphi_{bf} + \varphi\rho_p} \quad (7)$$

2.1.2 Thermal conductivity

The correlation of effective thermal conductivity presented by (Koo & Kleinstreuer, 2004) [21], and developed by (Vajjha & Das, 2009) [22]. This correlation consists of two parts, the first part is the static part and the second part is the dynamic part due to Brownian motion:

$$\eta_{eff} = \eta_{static} + \eta_{brownian} \quad (8)$$

Static thermal conductivity [23].

$$\eta_{static} = \eta_{bf}\left[\frac{(\eta_p+\eta_{bf})+2\varphi(\eta_p-\eta_{bf})}{(\eta_p+\eta_{bf})-\varphi(\eta_p-\eta_{bf})}\right] \quad (9)$$

Brownian thermal conductivity

$$\eta_{brownian} = 5\times10^4\beta\varphi\rho_{bf}C_{pbf}\sqrt{\frac{kT}{\rho_p d_p}}f(T,\varphi) \quad (10)$$

Where $k = 1.3807\times10^{-23}J/K$ is Boltzmann constant. Modeling function $f(T,\varphi)$ [7]

$$f(T,\varphi) = (2.8217\times10^{-2}\varphi + 3.917\times10^{-3})\left(\frac{T}{T_o}\right) + (-3.066910^{-2}\varphi - 3.91123\times10^{-3}) \quad (11)$$

2.1.3 Dynamic viscosity

Dynamic viscosity can be found from the formula [24]

$$\mu_{eff} = \mu_{bf}\times\frac{1}{\left(1-34.87\left(\frac{d_p}{d_{bf}}\right)^{-0.3}\times\varphi\right)} \quad (11)$$

Where μ_{eff} is the effective dynamic viscosity of nanofluid, μ_{bf} is the dynamic viscosity of the base-fluid, and d_{bf} is the equivalent diameter of the base fluid molecule is given by:

$$d_{bf} = 0.1\left[\frac{6M}{N\pi\rho_{bf}}\right]^{1/3} \quad (13)$$

Where M is the molecular weight of the base-fluid, N is the Avogadro number, and ρ_{bfo} is the mass density of the base-fluid estimated at the temperature $T_o = 293$ K. Thermophysical properties of base fluid (water) and Al_2O_3 nanoparticles used in this study are available in Table 1.

Table 1. Thermophysical properties of base fluid (water) and Al2O3 nanoparticles

Properties	Water	Al_2O_3
C_p (J / kg. K)	4179	765
ρ (kg/m^3)	997.1	4970
η *(W/m.K)*	0.613	40
μ (Pa.s)	$8.91\ x\ 10^{-4}$	–

3. Flow geometry and boundary conditions

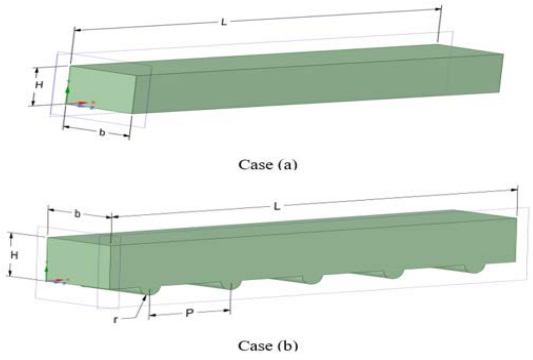

Figure 1. Computational domain. Case (a) straight channel, case (b) rectangular channel with half-circular grooves

Forced convection of turbulent nanofluid (Al_2O_3/ water) flow through a rectangular channel with a flat upper surface and the lower surface have grooves is studied by using the LES approach. The diagram of the computational domains is shown in Figure 1. The length of the channel (L) is (8H), the height of the channel (H) is 10 mm while the channel width (b) is (3/2 H). The radius of the half-circular groove (r) is 2 mm and the pitch (p) between the groove to another one is 16 mm. For the boundary conditions, the periodic boundary conditions are assigned in the spanwise and streamwise directions, and no-slip conditions are applied to both the upper flat wall and lower. For the thermal wall boundary conditions, the constant heat flux (5000 $/m^2$) is supplied to the upper and lower walls

4. Numerical approach

All the above-mentioned equations accompanied by boundary conditions are solved using finite volume method. The present set of nonlinear differential equations is discretized using the bounded central differencing method. The coupled pressure–velocity equation is solved by the SIMPLE algorithm. The bounded second-order implicit method is applied for the discretization of the time term. The time step size is set to $\Delta t = 2\ x\ 10^{-4}\ s$, and $t = 2\ s$ is considered for sampling time. Different distributions of the grid are

inspected to guarantee that the processed outcomes are grid-independent and the grid near the wall is sufficiently fine to determine the viscous sublayer effectively. The grid distributions for the four cases are given in T.able 1 at Re 5600 (equal to $Re_\tau = 180$.). Finer grid distribution may give more correct results, however, refinement of the precision of calculation will be little after the number of grid points is increased beyond a specific level, as demonstrated in Table 2.

Table2. Grid independence for at $Re_\tau = 590$.

No.	$N_x \, x \, N_y \, x \, N_z$	Nu
1	$120 \, x \, 60 \, x \, 60$	42.58451
2	$160 \, x \, 80 \, x \, 60$	42.6765
3	$160 \, x \, 80 \, x \, 70$	42.86568
4	$180 \, x \, 100 \, x \, 70$	43.1147
5	$200 \, x \, 120 \, x \, 90$	43.2034

The contrast is not conspicuous when the node numbers are greater than 1260000. Compared with the results of grid system No.3 and grid system No.4, the relative deviation of the Nusselt number is 0.2%. Therefore, it is concluded that an unequally spaced grid of 180 x 100 x 70 in the x, y, and z directions, consecutively, is adequate to describe the flow and heat transfer processes correctly.

5. Validation

The validation may be a major step in any numerical work in order to make sure that they're validated numerical code with other previous work, and it's ready for runs. For validation, the results obtained by simulation for a rectangular straight channel which included the variations of the dimensionless RMS of the three velocity components fluctuations for the present LES results compared with the DNS data of Moser et al. [16] for pure water, at Re= 5600 (equal to $Re_\tau = 180$). The dimensionless velocity fluctuations display acceptable accord with the DNS data [16], therefore the average deviation is 12.87% as shown in Figure 2. Subsequently, this work is dependable and it is able to foretell the mean and fluctuations of velocity and temperature of Al_2O_3/water nanofluid flow in a horizontal channel.

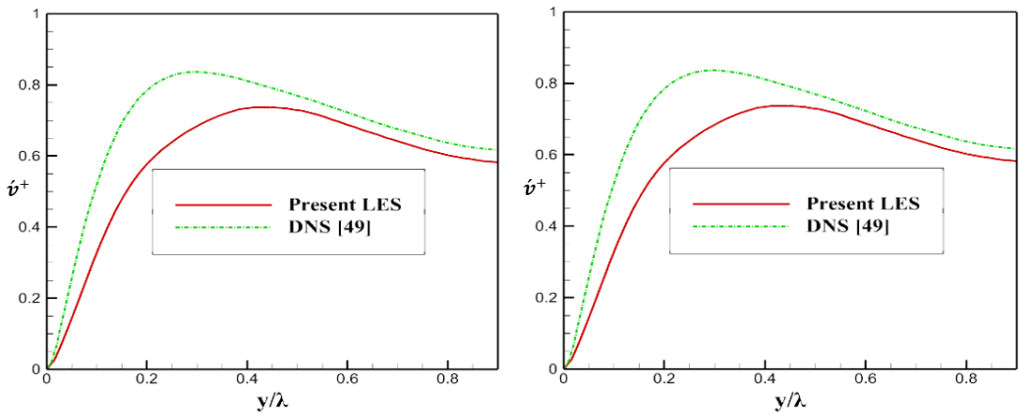

Figure 2. comparison of present LES results of pure water with Moser et [16]*al. data: (a)* $\acute{u}^+$*, (b)* $\acute{v}^+$

Results and discussion

The emulation and modelling of the fluid field and heat transfer of the nanofluid (Al_2O_3/ water) flow through a horizontal channel carried out for values of Re (Re =7000) and concentration of nanoparticles 0-4%. The results of mean value and fluctuations of velocity and temperature are presented across the channel spacing in the wall-normal direction (y), in the middle of the channel, at $x = 4H$ and $z = 3/4H$. The variations of the dimensionless mean velocity profiles in the wall-normal direction for $\varphi = 0 - 4\%$, at

Re (Re=700), are depicted in Figure 3. It observed that the presence of nanoparticles in the base fluid leads to a slight increase in the dimensionless mean velocity.

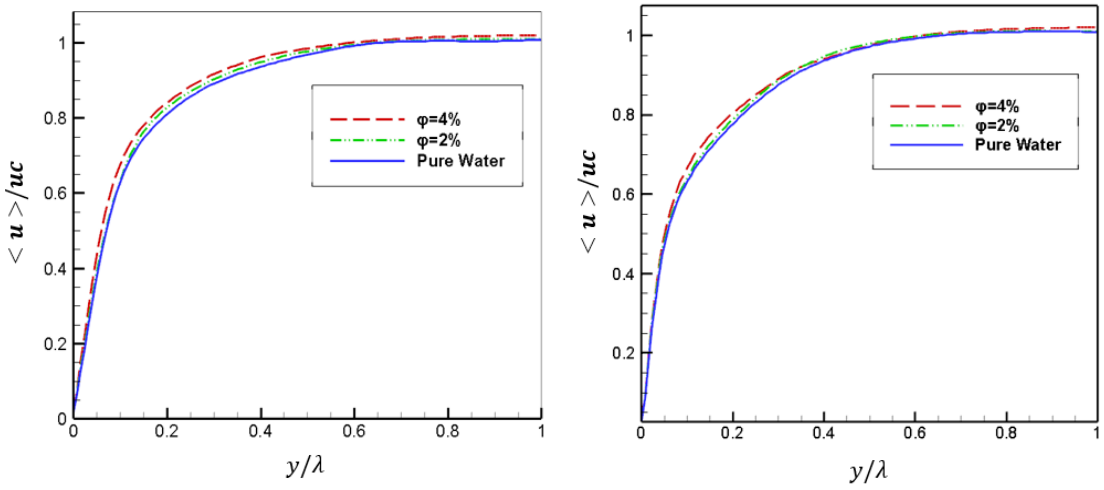

Figure 3 Variation of dimensionless mean velocity profiles in wall-normal direction for $\boldsymbol{\varphi = 0 - 4\%}$.

Figure 4 depicted the dimensionless RMS of turbulent velocity fluctuations profiles in the streamwise, wall-normal, and spanwise directions, at Re =7000. For the straight channel, the fluctuation in the streamwise direction is the largest one. However, the fluctuation in the spanwise direction is further up than fluctuation in the wall-normal direction. It implies that the stream is allowed to fluctuate more side-to-side rather than up and down, where the wall exerts an immediate restraint. While the presence of grooves led to a decrease in the fluctuation in the streamwise direction but the fluctuations in the wall-normal and spanwise direction in the straight channel in all cases. additionally, the results show that adding Al_2O_3 nanoparticles to the water (base fluid) increase the fluctuation in all directions and at Re.

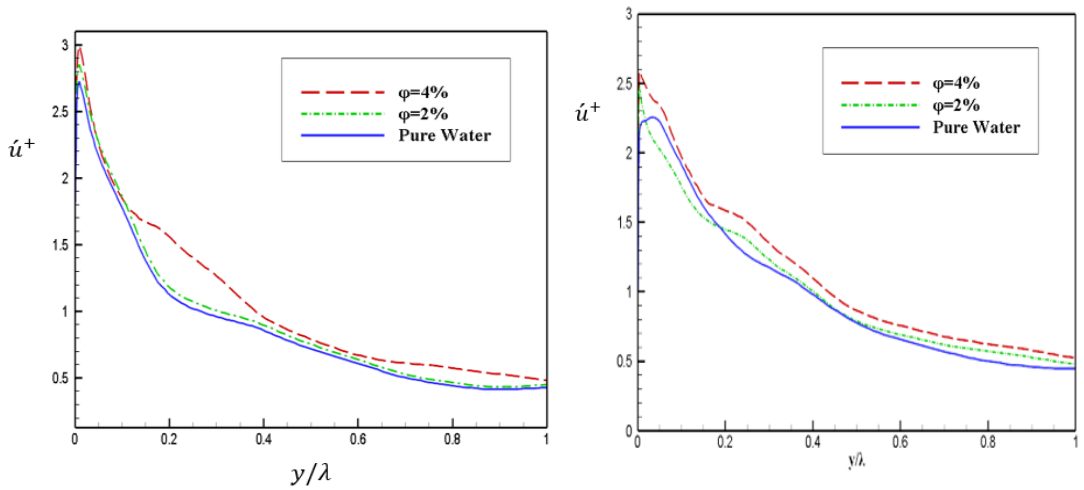

Figure 4. Distributions of dimensionless RMS of turbulent velocity fluctuations in wall-normal direction $\boldsymbol{\varphi = 0 - 4\%}$

Figure 5 describe the profiles of the dimensionless temperature fluctuations of water and nanofluid in the y-direction, the top value of temperature fluctuation $\left(T\acute{}^+ = \acute{T}/T_\tau\right)$ takes place in near-wall regions. presence of nanoparticles in a mix with the base fluid Leads to augment the top value of temperature fluctuations append nanoparticles of Al2O3 into the base fluid caused relatively higher temperature fluctuations. It

implies that higher energy transfer happens between the nanofluid layers giving a bigger measure of heat transfer than the pure water.

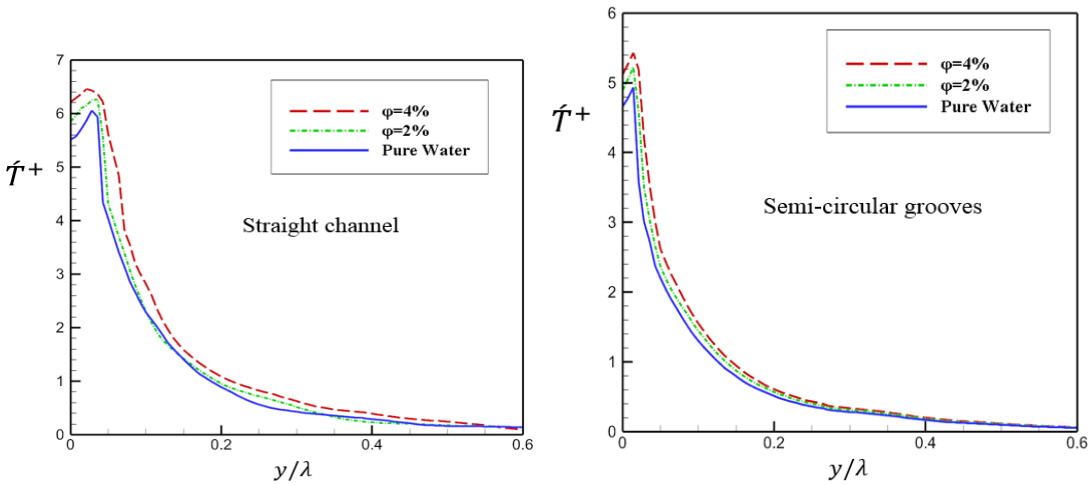

Figure 5. Profiles of dimensionless temperature fluctuations in wall-normal direction for $\boldsymbol{\varphi = 0 - 4\%}$

References

[1] M.R. Safaei, H. Togun, K. Vafai, S.N. Kazi, A. Badarudin, Investigation of heat transfer enhancement in a forward-facing contracting channel using FMWCNT nanofluids, Numer. Heat Transf. Part A Appl. 66 (2014) 1321–1340.

[2] M. Khoshvaght-Aliabadi, Influence of different design parameters and Al2O3-water nanofluid flow on heat transfer and flow characteristics of sinusoidal-corrugated channels, Energy Convers. Manag. 88 (2014) 96–105.

[3] V.A. Martínez, D.A. Vasco, C.M. García-Herrera, R. Ortega-Aguilera, Numerical study of TiO2-based nanofluids flow in microchannel heat sinks: Effect of the Reynolds number and the microchannel height, Appl. Therm. Eng. 161 (2019)

[4] S. Osman, M. Sharifpur, J.P. Meyer, Experimental investigation of convection heat transfer in the transition flow regime of aluminium oxide-water nanofluids in a rectangular channel, Int. J. Heat Mass Transf. 133 (2019) 895–902.

[5] R. Mashayekhi, H. Arasteh, D. Toghraie, S.H. Motaharpour, A. Keshmiri, M. Afrand, Heat transfer enhancement of Water-Al2O3 nanofluid in an oval channel equipped with two rows of twisted conical strip inserts in various directions: A two-phase approach, Comput. Math. with Appl. 79 (2020) 2203–2215.

[6] H.E. Ahmed, B.H. Salman, A.S. Kerbeet, Heat transfer enhancement of turbulent forced nanofluid flow in a duct using triangular rib, Int. J. Heat Mass Transf. 134 (2019) 30–40.

[7] W. Duangthongsuk, S. Wongwises, An experimental study on the heat transfer performance and pressure drop of TiO2-water nanofluids flowing under a turbulent flow regime, Int. J. Heat Mass Transf. 53 (2010) 334–344.

[8] B. Mehrjou, S. Zeinali Heris, K. Mohamadifard, Experimental study of CuO/water nanofluid turbulent convective heat transfer in square cross-section duct, Exp. Heat Transf. 28 (2015) 282–297.

[9] M. Parsaiemehr, F. Pourfattah, O.A. Akbari, D. Toghraie, G. Sheikhzadeh, Turbulent flow and heat transfer of Water/Al2O3 nanofluid inside a rectangular ribbed channel, Phys. E Low-Dimensional Syst. Nanostructures. 96 (2018) 73–84.

[10] M. Amani, P. Amani, A. Kasaeian, O. Mahian, W.M. Yan, Two-phase mixture model for nanofluid turbulent flow and heat transfer: Effect of heterogeneous distribution of nanoparticles, Chem. Eng. Sci. 167 (2017) 135–144.

[11] L. Davidson, Fluid mechanics, turbulent flow and turbulence modeling, (2015) 348.

[12] F. Bazdidi-Tehrani, S.I. Vasefi, A. Khabazipur, Scale-adaptive simulation of turbulent mixed convection of nanofluids in a vertical duct, J. Therm. Anal. Calorim. 131 (2018) 3011–3023.

[13] R.P. Worsnop, G.H. Bryan, J.K. Lundquist, J.A. Zhang, Using Large-Eddy Simulations to Define

Spectral and Coherence Characteristics of the Hurricane Boundary Layer for Wind-Energy Applications, Boundary-Layer Meteorol. 165 (2017) 55–86.
[14] J. Fröhlich, W. Rodi, Introduction to Large Eddy Simulation of Turbulent Flow, Endocr. Rev. 35 (2014) 267–298.
[15] A. Leonard, Energy cascade in large-eddy simulations of turbulent fluid flows, Adv. Geophys. 18 (1975) 237–248.
[16] R.D. Moser, J. Kim, N.N. Mansour, Direct numerical simulation of turbulent channel flow up to Reτ=590, Phys. Fluids. 11 (1999) 943–945.
[17] F. Nicoud, F. Ducros, Subgrid-scale stress modelling based on the square of the velocity, Agric. Econ. Res. Rev. 19 (2006) 37–48.
[18] F. Ducros, F. Nicoud, T. Poinsot, Wall-adapting local eddy-viscosity models for simulations in complex geometries, Conf. Numer. Methods Fluid Dyn. (1998) 1–7.
[19] Y.I.C. Bock Choon Pak, Hydrodynamic and Heat Transfer Study of Dispersed Fluids With Submicron Metallic Oxide, Exp. Heat Transf. A J. , Therm. Energy Transp. , Storage , Convers. (2013) 37–41.
[20] A. Adriana, Advances in Industrial Heat Transfer, 2012.
[21] J. Koo, C. Kleinstreuer, A new thermal conductivity model for nanofluids, J. Nanoparticle Res. 6 (2004) 577–588.
[22] R.S. Vajjha, D.K. Das, Experimental determination of thermal conductivity of three nanofluids and development of new correlations, Int. J. Heat Mass Transf. 52 (2009) 4675–4682.
[23] M. James Clerk, A treatise on electricity and magnetism, 9781108014 (2010) 1–442.
[24] M. Corcione, Heat transfer features of buoyancy-driven nanofluids inside rectangular enclosures differentially heated at the sidewalls, Int. J. Therm. Sci. 49 (2010) 1536–1546.